Mon. Not. R. Astron. Soc. 317, 687–696 (2000)

Angular diameter and effective temperature of a sample of 15 M giants at 2.2 μm from lunar occultation observations

Anandmayee Tej★ and T. Chandrasekhar
Astronomy and Astrophysics Division, Physical Research Laboratory, Navrangpura, Ahmedabad 380 009, India

Accepted 2000 May 8. Received 2000 April 18; in original form 2000 January 28

ABSTRACT
High angular resolution measurements of a sample of 15 M giants at 2.2 μm by the technique of lunar occultation are presented in this paper. We obtain angular diameters for 11 sources of which five are the first diameter measurements. For these resolved sources we have estimated the effective temperatures, which are consistent with previous calibrations. For the other four sources we put the first upper limits on their angular sizes to be 2 mas. Two sources, namely IRC+20090 and IRC+20067, yield appreciably low temperatures, which could point to their possible Mira nature. For sources with *Hipparcos* parallax measurements, we have calculated the linear radii.

Key words: occultations – stars: fundamental parameters – stars: late-type.

1 INTRODUCTION

Stars in the red giant phase occupy the cool end of the Herzsprung–Russell (HR) diagram. These are high-luminosity ($\sim$100–1000 $L_\odot$) stars spread over the spectral types G–M. M giant stars represent the major part of these red giant stars. M giants are relatively faint in the visible. Hence, compared with the early-type giants, they have not been the subject of intense scrutiny during the classical era of optical stellar astronomy. Extensive photometric and spectroscopic studies of M giants have been performed in recent years (Thé et al. 1990; Fluks et al. 1994), but there is still a dearth of high angular resolution (HAR) observations. One of the most challenging problems that still remains is the detailed study of the surface structure of these stars. With the advancement of the lunar occultation technique (Richichi et al. 1996, 1999a) and long-baseline interferometric methods (Perrin et al. 1998; van Belle et al. 1999) in the near-infrared (NIR), a large data base of angular diameters of these class of objects is now becoming available and hence a more focussed study of this group of stars is becoming possible.

The effective temperature of stars characterizes the radiometric properties of the stellar atmosphere. It is the measure of total energy, integrated over the entire spectrum, radiated from a surface of unit area. In the model computations of stellar atmospheres, the effective temperature is a fundamental parameter and, as one of the coordinates of the HR diagram, it plays an important role in the discussions of stellar evolution. The accurate determination of the effective temperature provides a decisive test for the relevance of various stellar models (Blackwell & Lynas-Gray 1994). The scale of temperatures of giants has been the target of a number of previous studies based on *direct* (angular diameter measurements) and *indirect* (from stellar atmosphere models) methods (Rigdway et al. 1980; Bell & Gustafsson 1990; Blackwell & Lynas-Gray 1998; Perrin et al. 1998; Alonso, Arribas & Martínez-Roger 1999; Richichi et al. 1999a; van Belle et al. 1999). Even though the effective temperature is fixed by the radius and luminosity of the star, the computation of its value from models is not straightforward as it is important to satisfy the physical criteria and the boundary values. T_{eff}, being a global property of the star, cannot in general be determined either from photometric colours or from atomic and molecular excitation. These methods give temperatures that are only indirectly related to the T_{eff}. Moreover, the spectra of M-type giants are severely affected by molecular absorption. Owing to strong molecular band opacities in the shorter wavelength region and longer wavelength infrared excess, the spectral energy distribution curve deviates significantly from that of a blackbody. Hence, the only direct means of obtaining the effective temperature of the star is from the measured angular diameter and the bolometric flux. From the basic definition it follows that

$$T_{\mathrm{eff}} = \left(\frac{4F}{\phi^2\sigma}\right)^{1/4}, \tag{1}$$

where F is the bolometric flux, which can be estimated from the multiwavelength photometry of the source, ϕ is the angular diameter and σ is the Stefan–Boltzman constant. This gives a hypothesis-free value of the T_{eff} that is completely independent of the distance to the star and hence is a powerful tool to test theoretical models on a large sample of stars. In this paper we describe the NIR lunar occultation observations and analysis of 15 M giants.

2 OBSERVATIONS AND DATA ANALYSIS

The lunar occultation observations of the sample of M giants were made with the 1.2-m telescope at Gurushikhar, Mount Abu

★ E-mail: tej@prl.ernet.in

Table 1. Predicted circumstances of the events for the M giant sample.

Source	Date of Observation	Event Type	Dewar Used	Time (UT) (hh mm ss)	Alt. of star (deg)	PA (deg)	CA (deg)	Vel. comp. (km s^{-1})
IRC−10305	1995 Mar 20	R	Fast	23 53 53	39.1	304.57	198.91	0.6746
IRC−20299	1995 Jun 11	D	Fast	18 29 33	45.3	96.12	−3.07	0.6807
IRC+10034	1995 Dec 04	D	Fast	16 08 35	71.7	108.92	40.81	0.4591
IRC+20090	1996 Feb 26	D	Fast	16 20 49	49.7	81.43	−9.53	0.6510
IRC+20111	1996 Feb 27	D	Fast	13 22 35	76.8	69.06	−16.72	0.5337
IRC−20444	1996 May 06	R	Fast	23 16 34	44.4	300.09	216.56	0.5333
IRC+10194	1996 May 23	D	Fast	15 34 35	36.1	104.32	−8.23	0.7557
IRC−10580	1996 Nov 18	D	Fast	16 16 39	39.7	76.52	12.89	0.7446
IRC+10038	1997 Jan 17	D	CVF	13 01 29	66.1	102.2	34.58	0.5343
IRC+20067	1997 Feb 14	D	CVF	17 07 04	37.1	60.59	−24.02	0.6945
IRC−10308	1998 Jan 22	R	CVF	01 32 37	52.0	310.00	18.7	0.571
IRC−10301	1995 Mar 20	R	Fast	19 52 26	44.2	297.39	183.02	0.7255
IRC−20470	1995 Mar 24	R	Fast	24 40 17	44.5	297.15	212.35	0.5395
IRC+20125	1995 Apr 06	D	Fast	14 56 56	49.6	115.69	14.70	0.6492
IRC+10032	1995 Dec 04	D	Fast	14 11 00	46.7	18.79	−49.09	0.4741

R – dark reappearance; D – dark disappearance; PA – position angle; CA – contact angle.

(72° 46′ 45.″9 E, 24° 39′ 10.″9 N; at 1680 m). Except for IRC−10308, the light curves were recorded with the single channel infrared fast photometer, which housed a liquid nitrogen cooled detector dewar. The details of the instrument can be found in Ashok et al. (1994). The journal of observations, the dewar used and the predicted circumstances of the events are listed in Table 1. The dewar with the circularly variable filter (CVF) is slower and hence the light curves recorded with this will appear to be more smoothened out in comparison with the ones obtained using the fast dewar. IRC−10308 was observed in the transmission channel of the dual channel infrared photometer (Mondal et al. 1999). We have recorded the time response of the detector system after each occultation event using a fast LED. This time-response curve is used in subsequent analysis. The cross identification of the sources are given in Table 2. Table 3 gives the source parameters. The spectral types listed in this table are compiled from literature.

Table 2. Cross identification for our M giant sample.

TMSS	SAO	*IRAS*	HD	Other Names
IRC−10305	158493	14165−1410	125357	MZ Vir
IRC−20299	159577	15527−1838	142521	–
IRC+10034	93196	02541+1424	18310	–
IRC+20090	–	04410+1752	–	–
IRC+20111	94604	0528+1831	36321	DV Tau
IRC−20444	–	18090−1853	–	–
IRC+10194	98143	08459+1243	75156	FX Cnc
IRC−10580	146043	22190−0751	212062	DZ Aqr
IRC+10038	–	03073+1315	–	ST Ari
IRC+20067	93659	0351+1527	–	–
IRC−10308	158929	14550−1214	132112	FY Lib
IRC−10301	158431	14104−1337	124304	EV Vir
IRC−20470	–	18197−1925	–	–
IRC+20125	94956	05502+1856	248740	–
IRC+10032	93166	02508+1427	17973	–

The data analysis procedure adopted is the standard iterative non-linear least-squares fitting procedure introduced by Nather & McCants (1970). We are able to reach a resolution limit of 2 mas for our angular diameter measurements. For resolved sources, the least-squares fitting procedure converges towards an angular diameter value that gives minimum χ^2. For an unresolved source ($\leqslant$2 mas in our case) the value of χ^2 remains flat up to the resolution limit and then increases monotonically with diameter. This χ^2 convergence test was performed for all of the sources and is presented in an inset in the figures showing the occultation light curves.

Table 3. Source parameters.

Source Name	RA (2000.0) (h m s)	Dec. (2000.0) (° ′ ″)	Spectral Type	*V*	*K*	*Hipparcos* Parallax(mas)
IRC−10305	14 19 14.9	−14 24 28.5	M1–M3 III	7.5	2.37	2.18 ± 0.98
IRC−20299	15 55 37.4	−18 47 27.9	M4 III	9.08	2.13	–
IRC+10034	02 56 52.2	+14 36 34.6	M4 III	8.71	1.28	–
IRC+20090	04 43 58.0	+17 58 12.0	M6	∼11	2.79	–
IRC+20111	05 31 06.3	+18 33 37.4	M6	8.4	1.35	–
IRC−20444	18 11 57.9	−18 52 14.0	M9	–	1.69	–
IRC+10194	08 48 39.5	+12 32 49.0	M3.3 III M3 III–II	6.8	1.87	2.24 ± 1.08
IRC−10580	22 21 41.8	−07 36 30.1	M7	8.52	0.47	3.51 ± 1.26
IRC+10038	03 10 07.8	+13 27 12.0	M4	9.0	2.37	–
IRC+20067	03 53 54.9	+15 36 41.5	M2	9.1	2.75	–
IRC−10308	14 57 46.5	−12 26 15.3	M5 III	7.1	0.15	2.97 ± 1.19
RC−10301	14 13 09.8	−13 51 35.8	M5 II M3 III M4.5 II–III	7.2	1.56	2.36 ± 1.20
IRC−20470	18 22 40.2	−19 23 35.0	M7	–	2.36	–
IRC+20125	05 53 08.8	+18 57 02.8	M5	8.70	2.75	–
IRC+10032	02 53 38.5	+14 40 12.9	M	7.58	2.64	1.57 ± 1.06

3 RESULTS

Of the 15 M giants chosen for detailed analysis we have resolved the stellar disc of 11 sources and have put an upper limit of 2 mas on the angular size of the other four. In this section we discuss the resolved sources by giving a brief history of each source as compiled from the literature and our results obtained.

3.1 Individual source details

3.1.1 *IRC−10305*

This star is classified as an M2/M3 giant. The infrared colours of this source are consistent with its spectral type. The light curve, along with the model fit to it, is shown in Fig. 1. It has been possible to find a good fit to the first three fringes, beyond which the scintillation noise dominates. We obtain a uniform disc (UD) angular size of 3.6 ± 0.2 mas. This is the first angular diameter measurement of this source. The derived effective temperature is 2883 ± 108 K. Using the recent *Hipparcos* parallax measurement of 2.18 ± 0.98 mas, we have derived a linear radius of $178 \pm 80\,R_{\odot}$.

In a recent work Lebzelter (1999) has mentioned an amplitude variation (~0.30 mag) seen in the *V* light curve of this source. Apart from this variation the light curve also shows lot of bumps and irregularities. A dual periodicity of 69 and 35 d is also obtained from the Fourier analysis of the light curve.

3.1.2 *IRC−20299*

This source is classified as M4 III. Based on the colours given in Perrin et al. (1998), the $V-K$ colour index assigns a spectral type of M6, but the $J-K$ and the $H-K$ colours suggest a spectral type closer to M8 for this source. Looking at the sensitivity of the colours to the spectral types we derive a spectral type of M7.5. We obtain a UD size of 3.1 ± 0.4 mas for this source. This is the first HAR observation of this source. The occultation light curve with the UD model fit to it is shown in Fig. 2. The effective temperature is derived to be 3140 ± 216 K. The spectral energy distribution of this source does not show any signature of an infrared excess.

3.1.3 *IRC+10034*

IRC+10034 is classified as M4 III by Lahulla (1987). The infrared colours of this source are similar to the colours of the previous source. The $V-K$ colour of 7.43 puts this source between M6 and M7, and the $J-K$ and the $H-K$ colours are close to M8. Based on this we give a spectral type of M7.5 for this source. We have a good quality light curve shown in Fig. 3. We

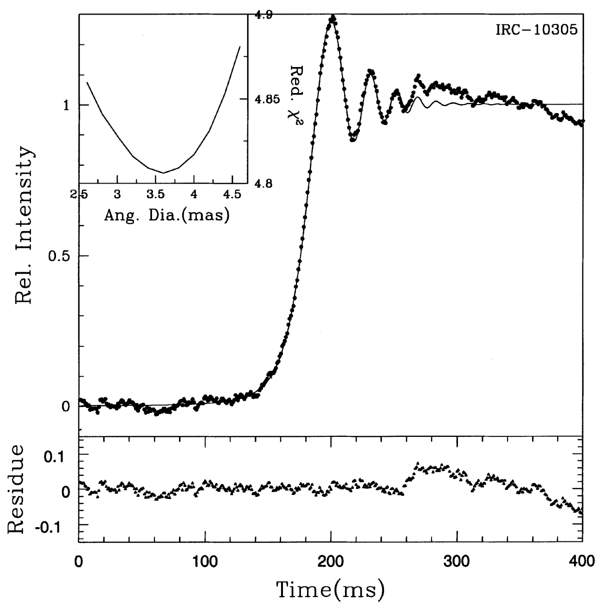

Figure 1. The data (filled circles) and the fitted model curve (solid line) for IRC−10305. The inset shows the χ^2 convergence. The lower panel shows the residuals of the fit (triangles).

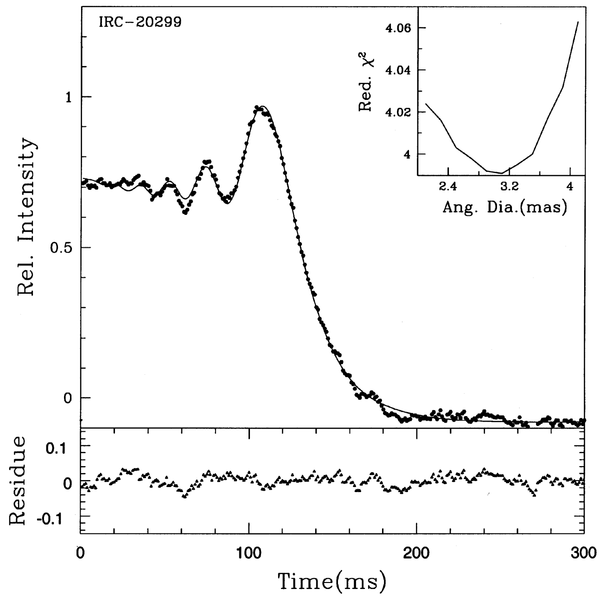

Figure 2. The data (filled circles) and the fitted model curve (solid line) for IRC−20299. The inset shows the χ^2 convergence. The lower panel shows the residuals of the fit (triangles).

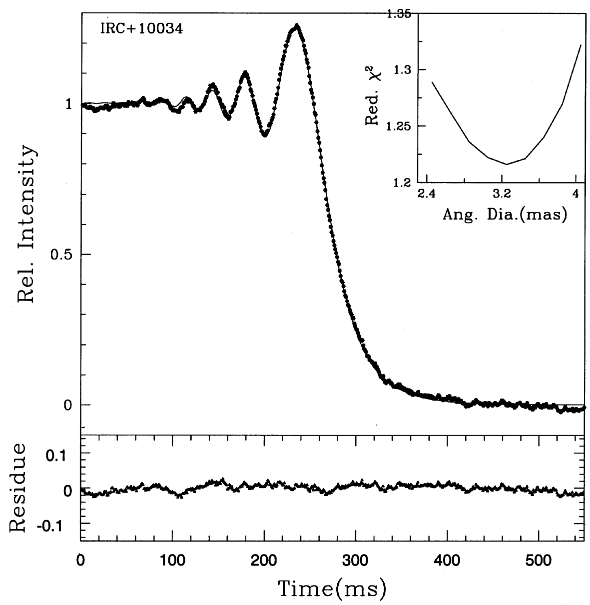

Figure 3. The data (filled circles) and the fitted model curve (solid line) for IRC+10034. The inset shows the χ^2 convergence. The lower panel shows the residuals of the fit (triangles).

obtain a UD angular diameter of 3.3 ± 0.3 mas for this source. This value of the UD diameter is consistent with that obtained by Richichi, Ragland & Fabbroni (1998a). They quote a value of 3.64 ± 0.07 mas. We derive an effective temperature of 3556 ± 186 K for this source.

3.1.4 IRC+20090

This source is classified as M6 (Bidelman 1980). This oxygen-rich giant has no previous angular diameter measurements. *JHK* and narrow band photometry by Noguchi (1989) show the signature of the strong 2.7-μm H_2O absorption band common to late-type stars with oxygen-rich envelopes. However, no infrared excess is seen from the flux distribution of this source. The light curve is shown in Fig. 4 We obtain a UD angular size of 3.7 ± 0.3 mas and a temperature of 2533 ± 123 K. This temperature is significantly low for this spectral type. However, our infrared colours place it in the Mira zone of the log T_{eff} versus $J - K$ plot of Feast (1996). As no accurate V magnitude is available, we have derived a spectral classification of M7.5 for this source based on the $J - K$ and the $H - K$ colour classification of Perrin et al. (1998). Further photometric and spectroscopic monitoring of this source will be very interesting.

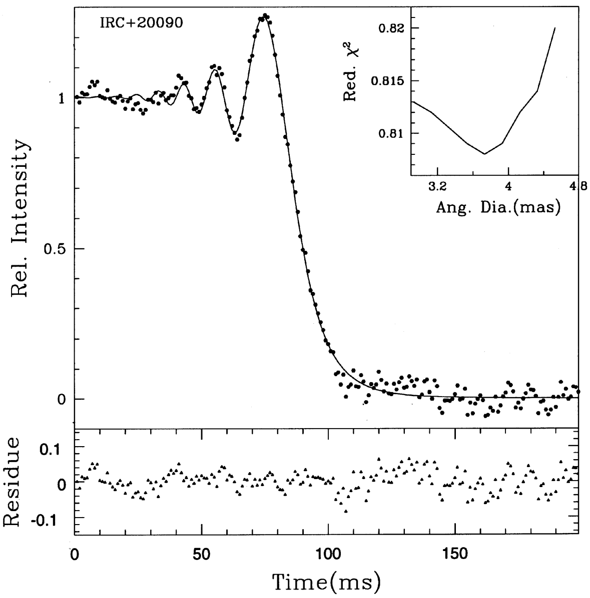

Figure 4. The data (filled circles) and the fitted model curve (solid line) for IRC+20090. The inset shows the χ^2 convergence. The lower panel shows the residuals of the fit (triangles).

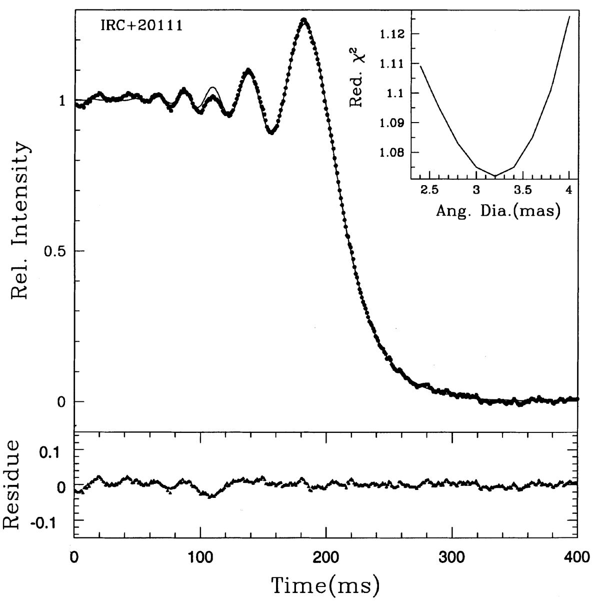

Figure 5. The data (filled circles) and the fitted model curve (solid line) for IRC+20111. The inset shows the χ^2 convergence. The lower panel shows the residuals of the fit (triangles).

3.1.5 IRC+20111

DV Tau is classified as M6 (Bidelman 1980). The *Infrared Astronomical Satellite* Low Resolution Spectrograph (*IRAS*-LRS) spectrum of this source is featureless. The data and the non-linear least-squares fit to it is shown in Fig. 5. We obtain a UD angular diameter value of 3.2 ± 0.4 mas. Earlier, Ridgway et al. (1982) resolved this source from lunar occultation observation at 1.618 μm. They obtained a UD value of 3.38 ± 0.19 mas. Richichi et al. (1998b) give a 2.2-μm angular diameter value of 3.79 ± 0.13 mas for IRC+20111. Within the quoted errors our value is consistent with these two measurements. We derive a temperature of 3318 ± 222 K, which is consistent with the temperature calibration for this spectral type. From the infrared colours we derive a spectral type of M7.5 for this source.

3.1.6 IRC−20444

Hansen & Blanco (1973) classify it as M8 or later. The other classification is M9 by Volk & Cohen (1989). The infrared colours $J - K$ and $H - K$ are 2.0 and 0.83, respectively, for this source, and these values place it beyond M8 in the colour classification (Perrin et al. 1998). We assign a spectral type of M9.5. This is the latest spectral type in our sample. The *IRAS*-LRS spectrum shows a broad 9.7-μm silicate emission feature and the spectral energy distribution shows an infrared excess in this source. From a previous lunar occultation of this source Richichi et al. (1998b) give a UD angular diameter of 4.54 ± 0.06 mas and an effective temperature of 2636 ± 132 K for this source. We obtain a UD value of 4.2 ± 0.5 mas. The data and the UD model fit to it is shown in Fig. 6. Uisng the bolometric flux listed in Richichi et al. (1998b) we derive an effective temperature of 2788 ± 215 K for this source. In a recent work Richichi et al. (1999b) reported the first detection of a companion around this source with a projected separation of 28 mas and a Δm of 2.8 mag. We do not see the signature of the companion in our light curve.

3.1.7 IRC+10194

This source is classified as M3.3 III by Kenyon & Fernandez-Castro (1987). The other classification found in the literature is M3 II–III (Keenan & McNeil 1989). There are several lunar occultation diameter measurements for this source. The journal of these previous values is given in Table 4. The light curve is shown in Fig. 7. We get a UD value of 3.0 ± 0.3 mas and an effective temperature of 3453 ± 244 K for IRC+10194. Within the errors this temperature is consistent with the spectral type M3 (Ridgway et al. 1980; Dyck, van Belle & Thompson 1998). The spectral classification of this source is consistent with the $V - K$ and $H -$

K colours, both of which give values for spectral type earlier than M5 based on colours given in Perrin et al. (1998). The $J - K$ colour, however, suggests a later spectral type but this index is not sensitive for spectral types earlier than M7. Hence, we derive a spectral type of M3.1 for this source.

The relatively large diameter value obtained for this source by Ridgway et al. (1980) and Ragland, Chandrasekhar & Ashok (1997) translated to low temperatures of 2810 ± 110 and 2760 ± 170 K, respectively. These temperature values, along with the infrared colours from Ridgway et al. (1980), displaced this source from the non-Mira M-type stars towards the Mira-type variables in the $\log T_{\rm eff}$ versus the $J - K$ colour plot of Feast (1996). Similar displacement was also seen in the $J - H$ versus $H - K$ diagram. However, this source is not a known Mira-type variable.

Our photometric colours and derived effective temperatures, however, place it in the non-Mira strip. This suggests that this source might have been a Mira in the past (Feast 1996) and leaves open the possibility of a real change in the star between the two epochs of observations.

From the *Hipparcos* parallax measurement of 2.24 ± 1.08 mas we derive a linear radius value of 144 ± 71 $R_\odot$ for this source.

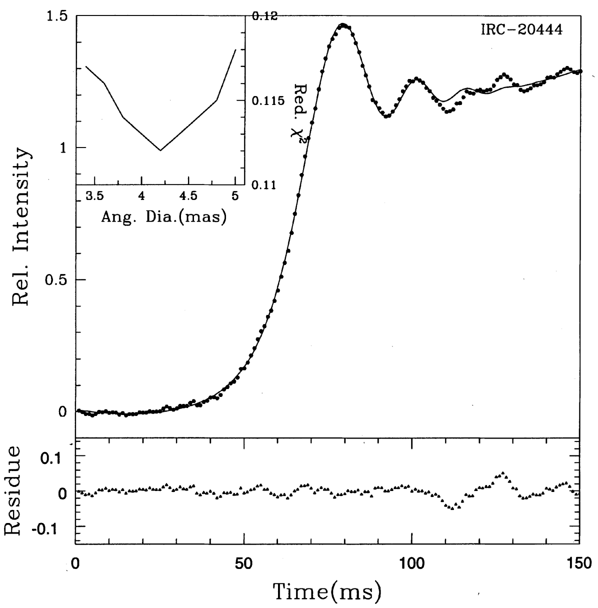

Figure 6. The data (filled circles) and the fitted model curve (solid line) for IRC−20444. The inset shows the χ^2 convergence. The lower panel shows the residuals of the fit (triangles).

Table 4. Journal of observations for IRC + 10194 and IRC − 10308.

Source	Year of Obsn	Wavelength of Obsn	$\phi_{\rm UD}$ (mas)	Refs
IRC+10194	1977	1.618 μm	4.49±0.59	1
	1976	1.640 μm	3.11±0.51	2
	1975	0.750 μm	4.00±0.50	3
	1994	2.200 μm	4.20±0.50	4
	1996	2.200 μm	3.00±0.30	*
IRC−10308	1979	1.618 μm	6.55±0.15	5
	1981	0.860 μm	6.69±0.07	5
	1981	1.618 μm	5.14±0.39	5
	1981	2.170 μm	5.49±0.37	5
	1981	1.650 μm	5.79±0.11	6
	1981	2.170 μm	5.80±0.20	6
	1998	2.200 μm	6.00±0.50	*

(1) Ridgway et al. 1979; (2) White 1978; (3) Ridgway, Wells & Joyce 1977; (4) Ragland et al. 1997; (5) Ridgway et al. 1982; (6) Schmidtke et al. 1986; * idicates results of this work.

3.1.8 IRC−10580

IRC−10580 is a semiregular oxygen-rich variable. Whitelock et al. (1995) list it as an M7 giant. The *IRAS*-LRS spectrum shows a strong and broad 10-μm emission feature. Hashimoto (1994) has fitted a radiative transfer model to the *IRAS* colours and the 10-μm silicate feature. He obtains an inner dust shell radius of $40R_*$ at a temperature of 465 K and an outer dust shell of radius $1000R_*$. Volk & Kwok (1987) derive a dust temperature of 515 K from the *IRAS* fluxes. From the model fitting of the 60- and 100-μm data to a central unresolved source surrounded by a resolved isothermal shell, Young, Phillips & Knapp (1993) have shown that DZ Aqr is not extended.

We get a UD value of 5.7 ± 0.4 mas. Fig. 8 shows the light curve and the model fit to it. No previous diameter estimate exists for this source. Radick & Lien (1980) mention a lunar occultation of IRC−10580, but have also remarked that the diameter of 9.6 ± 1.3 mas obtained from the analysis of their data is possibly spurious. We estimate an effective temperature of 3088 ± 134 K for this source. This temperature is consistent with the temperature derived for this spectral type by Perrin et al. (1998). The infrared colours are also consistent with the spectral type assigned to this source.

Using the recent *Hipparcos* parallax measurement for IRC−10580 of 3.51 ± 1.26 mas, we obtain a linear radius value of 175 ± 64 $R_\odot$.

3.1.9 IRC+10038

This star is of spectral type M4. It is classified as a semiregular variable of type SRb (Kerschbaum & Hron 1994). Jura & Kleinmann (1992) give a period of 99 d for IRC+10038 and a

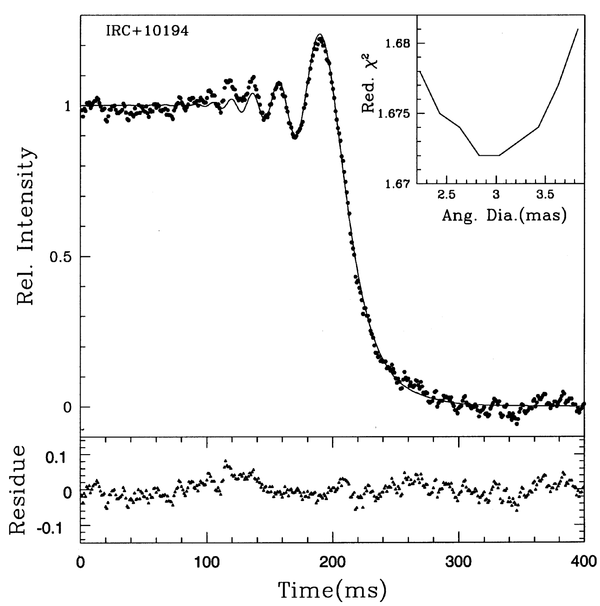

Figure 7. The data (filled circles) and the fitted model curve (solid line) for IRC+10194. The inset shows the χ^2 convergence. The lower panel shows the residuals of the fit (triangles).

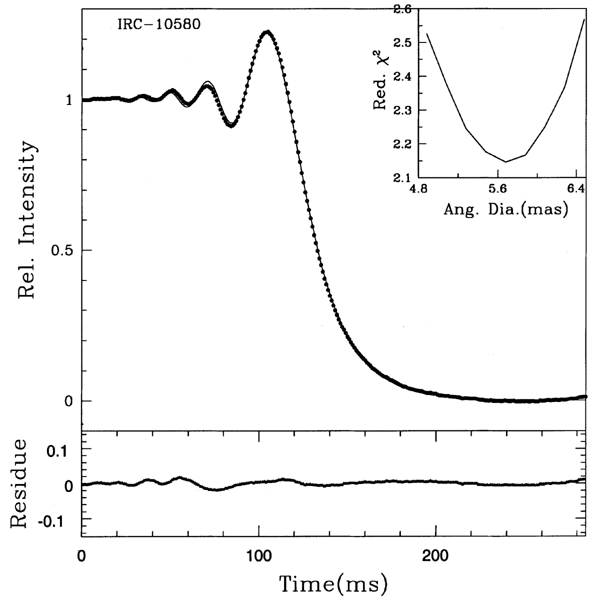

Figure 8. The data (filled circles) and the fitted model curve (solid line) for IRC−10580. The inset shows the χ^2 convergence. The lower panel shows the residuals of the fit (triangles).

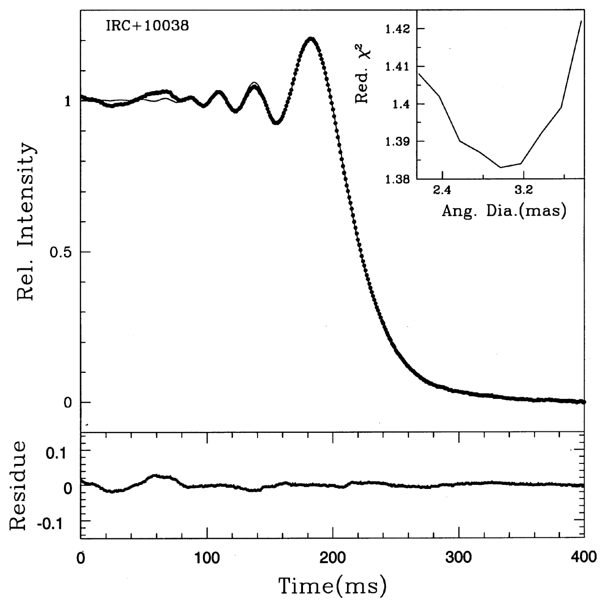

Figure 9. The data (filled circles) and the fitted model curve (solid line) for IRC+10038. The inset shows the χ^2 convergence. The lower panel shows the residuals of the fit (triangles).

visual magnitude of 9.0. A variability in the visual range of amplitude ~1.6 is also reported by them. The *IRAS* low resolution spectrum is featureless. The spectral energy distribution of this source shows an infrared excess. We have a good signal-to-noise ratio for the light curve. The data, along with the model fit to it, is shown in Fig. 9. We obtain an angular size of 3.0 ± 0.2 mas, which is the first diameter measurement for this source. We derive an effective temperature of 3098 ± 138 K. The infrared colour indices suggest a spectral type beyond M8 for this source. We adopt a spectral classification of M9 for this source.

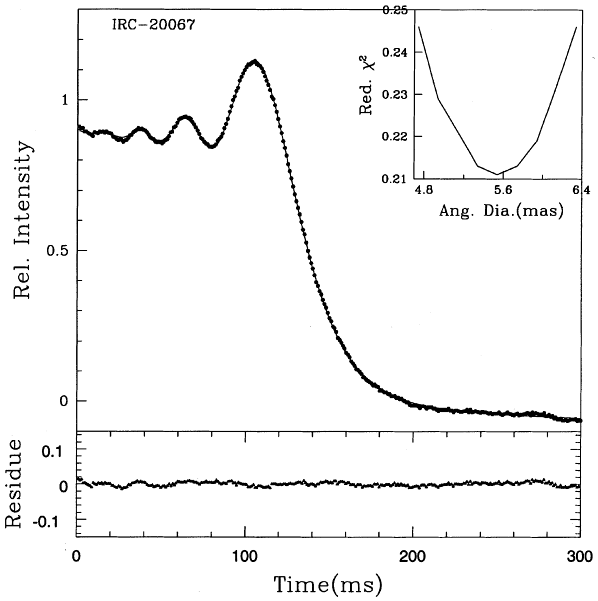

Figure 10. The data (filled circles) and the fitted model curve (solid line) for IRC+20067. The inset shows the χ^2 convergence. The lower panel shows the residuals of the fit (triangles).

3.1.10 IRC+20067

This source is classified as M2. Detailed data analysis yields a UD angular diameter of 5.4 ± 0.4 mas. The light curve and the model fit is shown in Fig. 10. Richichi et al. (1998b) quote a lower value of 3.68 ± 0.24 mas for the angular size of IRC+20067. We derive an effective temperature of 2244 ± 101 K. This temperature is appreciably low for this spectral type. However, the colour classification scheme of Perrin et al. (1998) puts this source at M7.5. In the $\log T_{\rm eff}$ versus $J-K$ colour index plot of Feast (1996), this source occupies a position in the Mira zone. Photometric monitoring of the source in the visible and NIR and NIR spectroscopy would help in understanding the nature of this source, i.e. whether it could be a Mira variable. The Mira nature of the source would adequately explain the lower temperature that was derived.

3.1.11 IRC−10308

This star is an oxygen rich semiregular variable of the type SRb. Noguchi (1990) classify it as M5 III. An alternate classification is of M3 by Stencel & Backman (1991). Hron, Aringer & Kerschbaum (1997) give an estimate of the stellar and dust temperature from blackbody fitting to the *IRAS*-LRS spectrum. They obtain a stellar and dust temperature of 2528 and 389 K, respectively. From his radiative transfer stellar model, Hashimoto (1994) gives an inner dust radius of $100R_*$ and an outer dust radius of $316R_*$. He derives a dust temperature of 289 K, whereas Volk & Kwok (1987) give a dust temperature of 728 K. The period of this variable is poorly defined. Jura & Kleinmann (1992) give a period of 120 d. A journal of previous lunar occultation results for this source is given in Table 4. Schmidtke et al. (1986) refer to a temporal variation in the size of IRC−10308 subject to position angle variation.

We obtain a UD value of 6 ± 0.5 mas. The data and the model fit is shown in Fig. 11. The infrared colours assign a spectral type of M7 to this source. We derive an effective temperature of

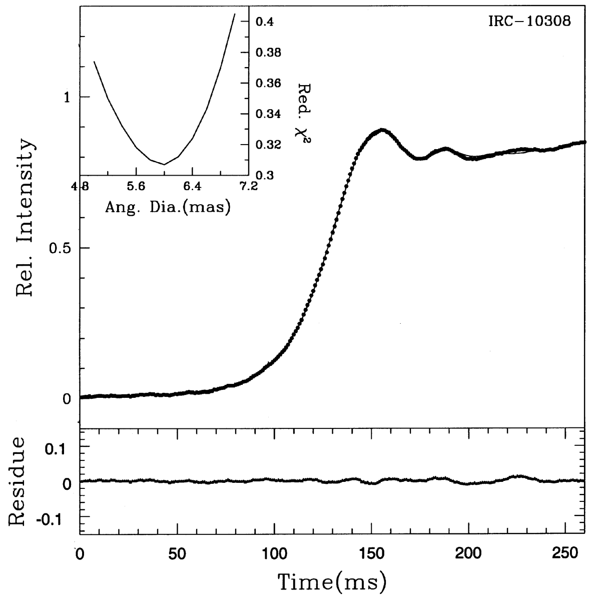

Figure 11. The data (filled circles) and the fitted model curve (solid line) for IRC − 10308. The inset shows the χ^2 convergence. The lower panel shows the residuals of the fit (triangles).

Table 5. Angular diameter results on M giants.

Source	ϕ_{UD} (mas)	ϕ_{LD} (mas)	Remarks
IRC−10305	3.6 ± 0.2	3.73	New
IRC−20299	3.1 ± 0.4	3.21	New
IRC+10034	3.3 ± 0.3	3.42	
IRC+20090	3.7 ± 0.3	3.83	New
IRC+20111	3.2 ± 0.4	3.31	
IRC−20444	4.2 ± 0.5	4.35	
IRC+10194	3.0 ± 0.3	3.11	
IRC−10580	5.7 ± 0.4	5.90	New
IRC+10038	3.0 ± 0.2	3.11	New
IRC+20067	5.4 ± 0.4	5.60	
IRC−10308	6.0 ± 0.5	6.21	
IRC−10301	⩽2.0	⩽2.07	New
IRC−20470	⩽2.0	⩽2.07	New
IRC+20125	⩽2.0	⩽2.07	New
IRC+10032	⩽2.0	⩽2.07	New

3160 ± 154 K. From the *Hipparcos* parallax measurement we obtain a linear radius of 217 ± 89 $R_\odot$.

3.2 Limb darkening

The derived UD diameters (ϕ_{UD}) are consolidated in Table 5. We have derived the diameter values of 11 sources out of which five are new diameter measurements. The four unresolved sources in our sample have no previous diameter measurements and hence we have put the first upper limits on the angular diameter of these sources. Limb darkening affects the measurements of stellar diameters of cool stars mostly at visual wavelengths, which are severely contaminated by molecular band absorption. Schmidtke et al. (1986) show that the effect of limb darkening in the NIR is typically around the 5 per cent level. Perrin et al. (1998) fitted their interferometric data with limb-darkened disc models (Manduca 1979; Scholz & Takeda 1987) in the *K* band in the

Table 6. Derived *JHK* magnitudes for our sample of M giants.

Source	JD	*J*	*H*	*K*
IRC−10305	245 0590.5	3.47 ± 0.03	2.63 ± 0.03	2.37 ± 0.03
IRC−20299	245 0590.5	3.46 ± 0.04	2.47 ± 0.03	2.13 ± 0.03
IRC+10034	245 0473.5	2.60 ± 0.03	1.65 ± 0.03	1.28 ± 0.03
IRC+20090	245 0482.5	4.16 ± 0.02	3.11 ± 0.03	2.79 ± 0.03
IRC+20111	245 0473.5	2.66 ± 0.03	1.72 ± 0.03	1.35 ± 0.03
IRC+10194	245 0916.5	3.04 ± 0.02	2.18 ± 0.03	1.87 ± 0.03
IRC−10580	245 0590.5	1.84 ± 0.02	0.85 ± 0.03	0.47 ± 0.03
IRC−10308	245 0919.5	1.44 ± 0.03	0.46 ± 0.03	0.15 ± 0.03
IRC−10301	245 0590.5	2.77 ± 0.03	1.85 ± 0.03	1.56 ± 0.03
IRC+20125	245 0473.5	3.96 ± 0.03	3.00 ± 0.03	2.75 ± 0.02
IRC+10032	245 0473.5	3.82 ± 0.03	2.90 ± 0.03	2.64 ± 0.03

3000–4500 K range. They suggested a scaling factor of 1.035 to obtain the limb-darkened diameter (ϕ_{LD}) from the UD value and this value has been adopted by us to calculate the limb-darkened diameters. These values are also listed in Table 5.

4 DISCUSSIONS

4.1 Bolometric flux

In spite of the relatively weak (power index of only 1/4) dependence of T_{eff} on the bolometric flux, as shown in equation (1), the accurate determination of the dependence is an important criteria for obtaining a reliable temperature scale. Bolometric fluxes are usually obtained by applying a bolometric correction to the measured *V* magnitude. However, this method fails for cool stars where the bolometric corrections are large and very sensitive to the spectral type. These cool stars radiate predominantly in the NIR, hence photometry in this critical spectral region where their flux distribution peaks helps in deriving the bolometric flux directly. We have carried out *JHK* photometry of most of the stars in our sample. The *JHK* magnitudes obtained by us are listed in Table 6. In the cases of the sources for which we failed to obtain an accurate *JHK* photometry, we have taken the magnitudes from the available literature. To complete the flux distribution curve we have taken the other optical and infrared magnitudes from reliable published sources. For the longer wavelength part of the curve we have consulted the *IRAS* Point Source Catalog and Gezari et al. (1993). We obtain the bolometric flux by either integrating from $\lambda = 0$ to $\lambda = \infty$ under the blackbody distribution curve, after matching with the observed flux at 2.2 μm, or by a simple trapezoidal rule. Both give consistent values. Ideally, one should have the bolometric flux at the same epoch of the angular diameter measurement as many of these sources are known to be variables. However, this has not always been possible. We have also used magnitude values that are spread over different epochs. Hence, the error in the bolometric flux includes the intrinsic variability of the source. The error is estimated to be typically 10 per cent.

Circumstellar extinction is present in some of the giants in our sample (e.g. IRC−10580). In this case the absorbed photospheric radiation is re-emitted locally and shows up in the spectral energy distribution as an infrared excess. A blackbody model is fitted to this excess and added to the total stellar flux to obtain the original bolometric flux from the photosphere. Fig. 12 shows the spectral energy distribution for a sample of four M giants. The bolometric fluxes estimated for the resolved sources are listed along with the derived effective temperatures in Table 7.

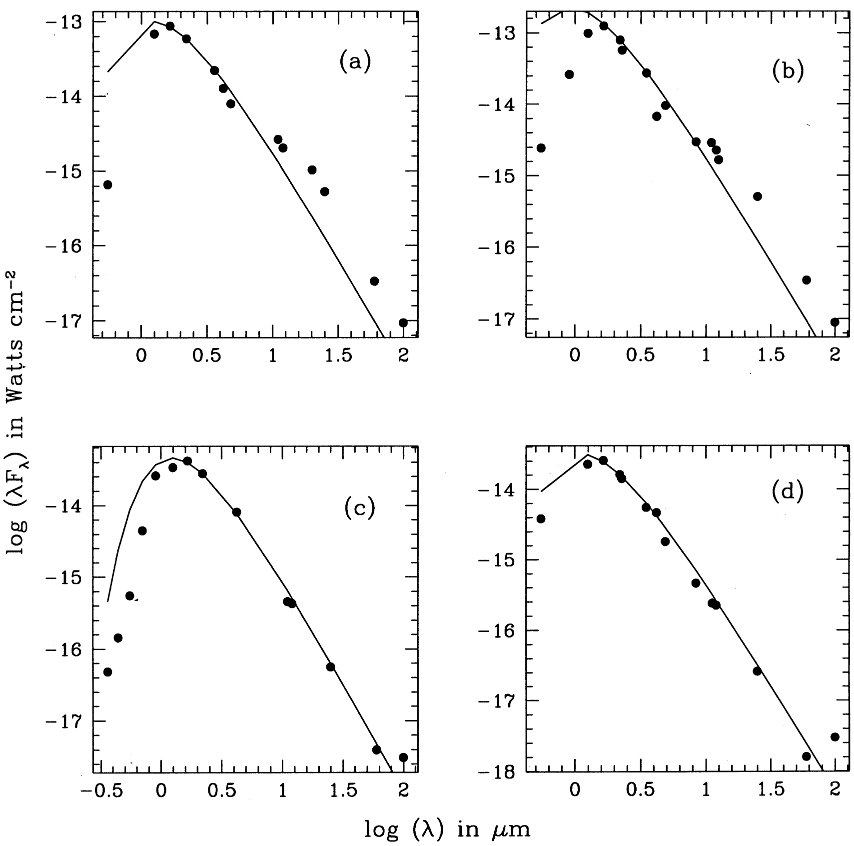

Figure 12. The spectral energy distribution of (a) IRC−10580 (b) IRC−10308 (c) IRC+10034 and (d) IRC+10194. IRC−10580 and IRC−10308 show signatures of infrared excess.

Table 7. Effective temperatures of the resolved M giants.

Source	Spec. Type (derived)	$V-K$	$J-K$	Bol. Flux ($\times10^{-14}\,\mathrm{W\,cm^{-2}}$)	T_{eff} (K)
IRC−10305	M2.0	5.13	1.10	2.98	2883 ± 108
IRC−20299	M7.5	6.95	1.33	3.11	3140 ± 216
IRC+10034	M7.5	7.43	1.32	5.80	3556 ± 186
IRC+20090	M7.5	8.21	1.37	1.88	2533 ± 123
IRC+20111	M7.5	7.05	1.31	4.13	3318 ± 222
IRC−20444	M9.5	10.31	2.0	3.55	2788 ± 215
IRC+10194	M3.1	4.93	1.17	4.26	3453 ± 190
IRC+10038	M9.0	6.63	1.68	2.76	3098 ± 133
IRC+20067	M7.5	6.35	1.34	2.46	2244 ± 101
IRC−10580	M7.0	8.05	1.37	9.84	3088 ± 134
IRC−10308	M7.0	6.95	1.29	11.95	3160 ± 154

4.2 The effective temperature and uncertainty in the spectral classification of M giants

Initially, lunar occultation and, more recently, long baseline interferometry results have contributed towards the accumulation of reliable angular diameter values, which enables the derivation of accurate effective temperatures of M giants and the establishment of a calibration between the spectral type and the effective temperatures of this group of stars. Ridgway et al. (1980) were the first to give the temperature calibration from K0 to M6 based on NIR lunar occultation diameter measurements. Temperature estimations from long baseline interferometry (Di Benedetto & Rabbia 1987; Dyck et al. 1998; Perrin et al. 1998 and van Belle et al. 1999) form a large data base that is consistent with the calibration of Ridgway et al. (1980), and extends well this occultation data law beyond M6. A homogeneous temperature calibration, ensuring uniformity in the details of data acquisition and analysis, has been recently reported by Richichi et al. (1999a). It is based on lunar occultation diameters at 2.2 μm. The effective temperatures calculated for our sample from our measured angular diameters and the estimated bolometric fluxes are listed in Table 7. In order to obtain a well defined spectral class versus temperature calibration one requires accurate spectral classification of the sources under study, which is usually not available. Discrepancies such as multiple classification for the same star, inconsistency with the observed colours or inaccuracy of the original source of classification are seen. The difficulties encountered in deriving an accurate classification are usually:

(1) a lack of proper standards;
(2) variability of the source;
(3) in the range K4–M1, TiO bands just begin to become visible and can be confused with nearby groups of atomic lines unless very high dispersion is used;
(4) the absorption bands of TiO become very strong beyond M4, hence it becomes difficult to find stretches of continuum where atomic lines can be reliably compared;
(5) early M-type stars also have problems of TiO line blanketing.

Moreover, all these classifications are based on observations restricted to the visual or very NIR ($\sim$1.06 μm). For M giants this part of the spectrum is not suitable because the continuum is high, the line opacity effects are large and also because this region lies on the exponential part of the Planck's curve and is quite sensitive to temperature. Perrin et al. (1998) use the infrared colours based on photometry in bands redder than *J* as stable indicators of the spectral types. They have estimated the intrinsic colours for the spectral range M5–M8 derived from a sample of bolometrically bright giants. Based on these colours we have attempted to reclassify the sources in our sample. The derived spectral types are listed in Table 7.

In Fig. 13 we have plotted effective temperatures as a function of the spectral types derived for the M giants in our sample. The uncertainties involved in the derivation of the spectral types are shown as error bars. It can be seen that there is a clustering of our results around M7–M8. To compare our results with previous temperature calibrations, we have also plotted the model curves derived by different groups in Fig. 13. As can be seen, the temperatures derived for eight sources, namely IRC−20299, +10034, +20111, −20444, +10194, +10038, −10580 and −10308, are consistent with previous calibrations. Two sources (IRC + 20090 and +20067), which could be of Miras type, yield low temperatures. IRC−10305 also gives a lower temperature.

As short period variability is common to most M giants (Lebzelter 1999), continuous monitoring of these sources is necessary to arrive at a meaningful temperature scale. The uncertainty in the spectral classification also makes it difficult to get a well-defined calibration of the temperature versus the spectral type for late M sources. The use of spectral features in the 1.0–3.0-μm region can give a more reliable classification. Opacities being less, emission from a deeper and more stable part of the atmosphere can be sampled. This spectral region offers strong absorption lines, such as the CO overtone bands, Fe I, Na I doublets, Ca I triplet, Mg I etc., as stable spectral-type indicators. However, there is still no consensus in the literature on spectral typing based on infrared high-resolution spectra and, clearly, further study is needed in this direction.

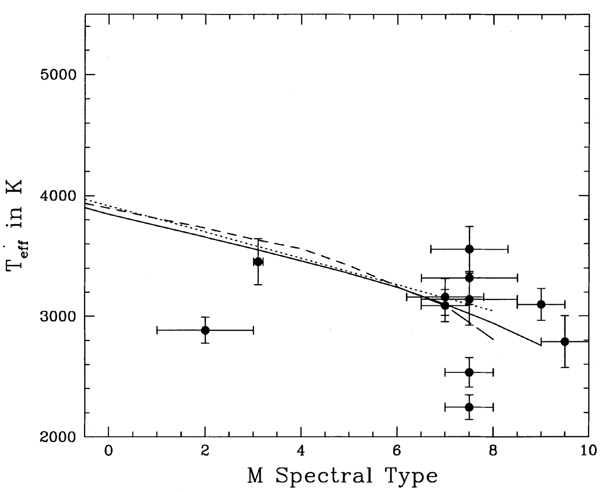

Figure 13. This figure compares our data points with all the other effective temperature calibrations from the literature. The fitted curves obtained by different groups are as follows: Richichi et al. (1999a – solid line); van Belle et al. (1999 – dotted line); Ridgway et al. (1980 – short-dashed line) and Perrin et al. (1998 – long-dashed line).

5 CONCLUSION

Using the technique of lunar occultation we have derived the angular diameters of a sample of 15 M giants. Of these, 11 sources have well-resolved stellar discs in the range 3–6 mas and we give the first HAR measurements for five of them. For the other four sources we put the first upper limit on their size to be 2 mas. Except for two sources, namely IRC+20090 and IRC+20067, which show appreciably low temperatures, the effective temperatures calculated are consistent with previous calibrations. As many of the later M types are variable sources, multiple HAR observations and bolometric flux determinations of each of these sources are required before one can derive its effective temperature accurately. A reliable spectral classification based on infrared spectroscopy is also essential to derive a meaningful temperature scale for M giants.

ACKNOWLEDGMENTS

This work was supported by Department of Space of the Government of India. The authors wish to thank the referee for his useful comments.

REFERENCES

Alonso A., Arribas S., Martínez-Roger C., 1999, A&AS, 139, 335
Ashok N. M., Chandrasekhar T., Ragland S., Bhatt H. C., 1994, Exp. Astron., 4, 177
Bell R. A., Gustafsson B., 1990, MNRAS, 236, 653
Bidelman W. P., 1980, Publ. Warner Swasey Obs., 2, 6
Blackwell D. E., Lynas-Gray A. E., 1994, A&A, 282, 899
Blackwell D. E., Lynas-Gray A. E., 1998, A&AS, 129, 505
Di Benedetto G. P., Rabbia Y., 1987, A&A, 188, 114
Dyck H. M., van Belle G. T., Thompson R. R., 1998, AJ, 116, 981
Feast M., 1996, MNRAS, 278, 11
Fluks M. A., Plez B., Thè P. S., de Winter D., Westerlund B. E., Steenman H. C., 1994, A&AS, 105, 311
Gezari D. Y., Schmitz M., Pitts P. S., Mead J. M., 1993, Catalog of Infrared Observations, 1294, NASA Ref. Publ.
Hansen O. L., Blanco V. M., 1973, AJ, 78, 669
Hashimoto O., 1994, A&AS, 107, 445
Hron J., Aringer B., Kerschbaum F., 1997, A&A, 322, 280
Jura M., Kleinmann S. G., 1992, ApJS, 83, 329
Keenan P. C., McNeil R. C., 1989, ApJS, 71, 245
Kenyon S. J., Fernandez-Castro T., 1987, AJ, 93, 938
Kerschbaum F., Hron J., 1994, A&AS, 106, 397
Lahulla J. F., 1987, PASP, 99, 998
Lebzelter T., 1999, A&A, 346, 537
Manduca A., 1979, A&AS, 36, 411
Mondal S., Chandrasekhar T., Ashok N. M., Kikani P. K., 1998, Bull. Astron. Soc. India, 27, 335
Nather R. E., McCants M. M., 1970, AJ, 75, 963
Noguchi K., 1989, PASJ, 41, 779

Noguchi K., 1990, PASJ, 42, 419
Perrin G., Coudé du Foresto V., Ridgway S. T., Mariotti J. M., Traub W. A., Carleton N. P., Lacasse M. G., 1998, A&A, 331, 619
Radick R., Lien D., 1980, AJ, 85, 1053
Ragland S., Chandrasekhar T., Ashok N. M., 1997, MNRAS, 287, 681
Richichi A., Ragland S., Fabbroni L., 1998a, A&A, 330, 578
Richichi A., Baffa C., Calamai G., Lisi F., 1996, AJ, 112, 2786
Richichi A., Ragland S., Stecklum B., Leinert Ch., 1998b, A&A, 338, 5, 27
Richichi A., Fabbroni L., Ragland S., Scholz M., 1999a, A&A, 344, 511
Richichi A., Ragland S., Calamai G., Baffa C., Stecklum B., Richter S., 1999b, A&A, 350, 491
Ridgway S. T., Wells D. C., Joyce R. R., 1977, AJ, 82, 414
Ridgway S. T., Wells D. C., Joyce R. R., Allen R. G., 1979, AJ, 84, 247
Ridgway S. T., Joyce R. R., White N. M., Wing R. F., 1980, ApJ, 235, 126
Ridgway S. T., Jacoby G. H., Joyce R. R., Siegel M. J., Wells D. C., 1982, AJ, 87, 808
Schmidtke P. C., Africano J. L., Jacoby G. H., Joyce R. R., Ridgway S. T., 1986, AJ, 91, 961
Scholz M., Takeda Y., 1987, A&A, 186, 200
Stencel R. E., Backman D. E., 1991, ApJS, 75, 905
Thè P. S., Thomas D., Christensen C. G., Westerlund B. E., 1990, PASP, 102, 565
van Belle G. T., Lane B. F., Thompson R. R., Boden A. F., 1999, AJ, 117, 521
Volk K., Cohen M., 1989, AJ, 98, 931
Volk K., Kwok S., 1987, ApJ, 315, 654
White N. M., 1978, in Philip A. G. D., Hayes D. S., eds, Proc. IAU Symp. 80, The HR Diagram. Davis Press, Schenectady, New York, p. 447
Whitelock P., Menzies J., Feast M., Catchpole R., Marang F., Carter B., 1995, MNRAS, 276, 219
Young K., Phillips T. G., Knapp G. R., 1993, ApJS, 86, 517

This paper has been typeset from a TEX/LATEX file prepared by the author.